DE GRUYTER OPEN

Acta Geophysica
vol. 64, no. 6, Dec. 2016, pp. 2591-2608
DOI: 10.1515/acgeo-2016-0101

Imprints of Natural Phenomena and Human Activity Observed During 10 Years of ELF Magnetic Measurements at the Hylaty Geophysical Station in Poland

Zenon NIECKARZ

Institute of Physics, Jagiellonian University, Kraków, Poland;
e-mail: zenon.nieckarz@uj.edu.pl

A b s t r a c t

Current human activity produces strong electromagnetic pollution. The power spectrum in the extremely low frequency (ELF, 3-3000 Hz) range is mainly polluted by anthropogenic narrow spectral lines at 16.66, 50, and 60 Hz and their harmonics. Meanwhile, signatures connected with natural phenomena appearing in the Earth's atmosphere, ionosphere and magnetosphere are also observed in the same frequency range.

This paper presents the amplitude behaviour of the anthropogenic lines in the years 2005-2014 based on the 10 years of activity of the Hylaty station situated in southeast Poland. The analysis includes, *i.a.*, an assessment of the correctness of the choice of the Bieszczady mountains as a location for the installation of an ELF station for long-term geophysical and climatological studies.

Key words: electromagnetic pollution, human activity, ELF waves.

1. INTRODUCTION

The measurement of magnetic field components in the frequency domain from nearly DC to a few hundred Hertz at stations located on the surface of the Earth is a widely used method in geophysical, meteorological, climatological, and earth science studies. Different signatures of the following phenomena are observed in the records obtained: structured and unstructured pearl pulsation (Pc1) elicited by geomagnetic storms, spectral resonance structures (SRS) associated with activity in the Alfvén resonator (IAR), and Schuman resonances (SchR) connected with lightning activity inside the Earth-ionosphere (E-i) cavity.

Measurements of ELF waves are performed in several regions of the world: in the USA at Hollister (36.8°N, 121.5°W) and Rhode Island (41.6°N, 71.6°W); in Israel at Mitzpe-Ramon (30.5°N, 34.4°E); in Japan at Moshiri (142.2°E, 44.3°N); in Russia at Lekhta (33.9°E, 64.4°N), and Vernadsky (65.3°S, 64.2°W); and the Ukrainian ELF station at Antarctica. General and detailed descriptions are available in many papers (Fraser-Smith and Helliwell 1994, Price *et al.* 1999, Hobara *et al.* 2000, Bezrodny *et al.* 2007). In Europe a few stations also work continuously, such as Nagycenk (47.6°N, 16.7°E) in Hungary, and Eskdalemuir in United Kingdom (55.314°N, 3.206°W), which are described in detail in papers (Sátori *et al.* 1996, Beggan *et al.* 2012). Most of these stations correctly measure the signals at frequencies below 3 Hz, which fall within the ULF (ultra low frequency) range. It should be noted that the ULF wave range is widely used in geophysics studies, *i.e.*, by INTERMAGNET Magnetic Observatories, which use sampling intervals of one or a few seconds to observe Earth's magnetic field (Jankowski and Sucksdorff 1996, Love and Chulliat 2013, Turbitt *et al.* 2013).

Two centres in Poland perform measurements of ELF waves. One of them is the Institute of Geophysics, Polish Academy of Sciences, which founded two ELF stations (Neska and Sátori 2006), one in the Polish Polar Station at Spitsbergen (77.0°N, 15.5°E) and second in the Central Geophysical Observatory in Belsk (51.8°N, 20.8°E). The other centre is the Astronomical Observatory of the Jagiellonian University in Kraków, which has provided continuous ELF measurements at the Hylaty ELF station since 2006. The station is situated in southeast Poland (Bieszczady Mountains, 49.2°N, 22.5°E). The data are gathered and shared by Cracow ELF Group (Kulak *et al.* 2014).

The aim of this paper is to look at ELF signals recorded in Hylaty station for identification and characterization of anthropogenic traces as well as for analysing their influence on the quality of study of the natural terrestrial and extra-terrestrial sources of signals.

2. DATA SET

In this paper, data collected by the Hylaty ELF station have been used. Figure 1 shows the location of the Hylaty ELF station. The geographic and geomagnetic coordinates are (49.2°N, 22.5°E) and (44.6°N, 96.8°E), respectively and the *L*-shell parameter is 1.98. Figure 2 shows the block diagram of the station. It contains a receiver and antennae. The receiver is placed in an underground container. Two orthogonal magnetic antennae are placed about 100 m away and oriented in the North-South and East-West directions. The EM waves are transversal in nature and their ELF range propagates within the Earth-ionosphere cavity. For this reason, the magnetic antenna positioned along the EW axis has the highest reception sensitivity to waves propagating along the NS axis and, by analogy, the antenna positioned along the NS axis receives best the waves propagating along the EW axis, as predicted by the Hertz dipole's directional reception characteristic.

The antennae are 1 m long and are designed as active magnetic antennae powered by the receiver unit. The station produces 2.5 MB of data per hour with a sampling frequency of 175 Hz and a dynamic range of 16 bits, and has the 3 dB frequency bandwidth of 0.03 to 55 Hz. More details of this station are described by Kulak *et al.* (2014).

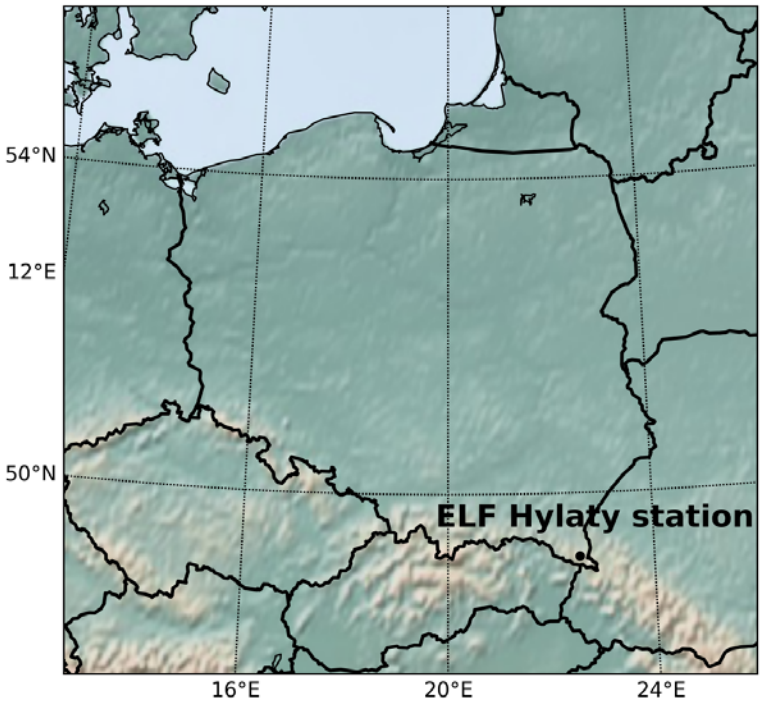

Fig. 1. Map showing the location of the ELF station in Poland.

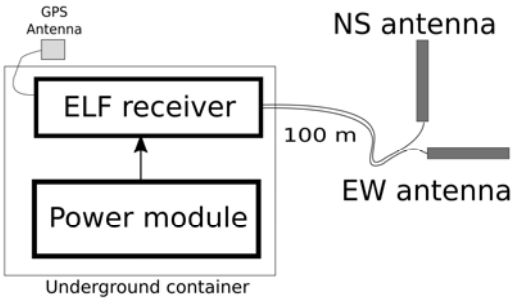

Fig. 2. Block diagram of the Hylaty ELF station.

Data sets from two magnetic antennae and a thermometer inside an underground container have been collected during the station's ten years of operation. Figure 3 (solid line) presents the variability of the daily average temperature during the years 2005-2014. The lowest instantaneous value of temperature was not colder than +1.4°C. The daily average minimum (+1.4°C) and maximum (+16.6°C) temperatures were recorded during the days 19-23 February 2012 and 1-4 August 2005, respectively. The average temperature for all ten years was 7.9 ± 4.2°C.

The nearest station to Hylaty in Poland is operated by the Institute of Meteorology and Water Management and is located at Lesko at a distance of 36 km. The data are available via FTP protocol: ftp://ftp.ncdc.noaa.gov/pub/data/gsod. The change of daily air temperature measured by this hydrological and meteorological station is shown in Fig. 3 (as dots). The close correlation between both sets of temperatures is clearly visible.

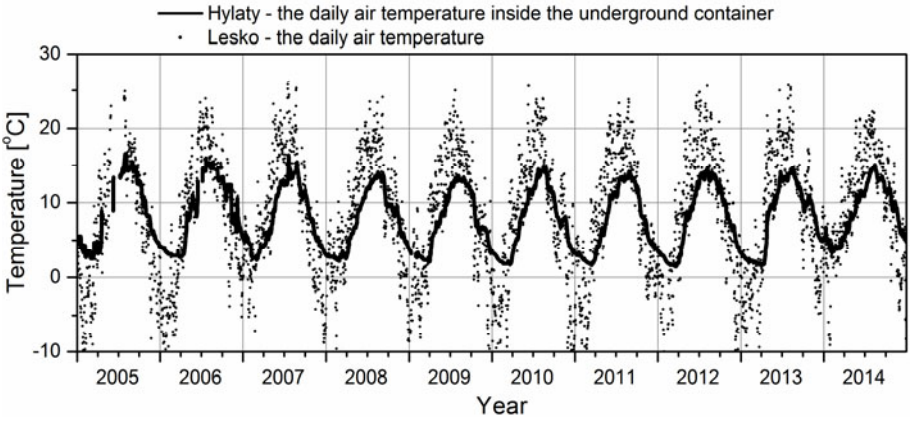

Fig. 3. The variation of the daily air temperature at Lesko (dots) and the daily air temperature inside the underground container (line) during the 10-year period (2005-2014).

The annual maximum and minimum air temperatures in Lesko were earlier than in the temperatures recorded by the ELF station and this response is expected in accordance with general scientific principles (Salazar 2006). The location of the ELF receiver in an underground chamber prevents the temperature from lowering below zero degrees Celsius and the device freezing. This effect achieves what is confirmed by Fig. 3. Daily temperature variations are not observed inside the container.

3. ULF/ELF SIGNATURES OF NATURAL PHENOMENA

3.1 Pc1 and Pi1 pulsations

Extensive study of the dynamic power spectrum calculated from magnetic field components allows one to distinguish the signatures of the different natural phenomena mentioned in the introduction. In the lower part of the frequency domain of the power spectrum, a signature connected with processes in the Earth's magnetosphere and solar wind is observed. Solar flares and related plasma injections into the Earth's magnetosphere causing the intensification of current circuits are commonly thought to be responsible for the waves registered by magnetometers (Engebretson *et al.* 2008). Oscillations with quasi-sinusoidal waveform were called pulsations continuous (Pc1) and those with waveforms that are more irregular are called pulsations

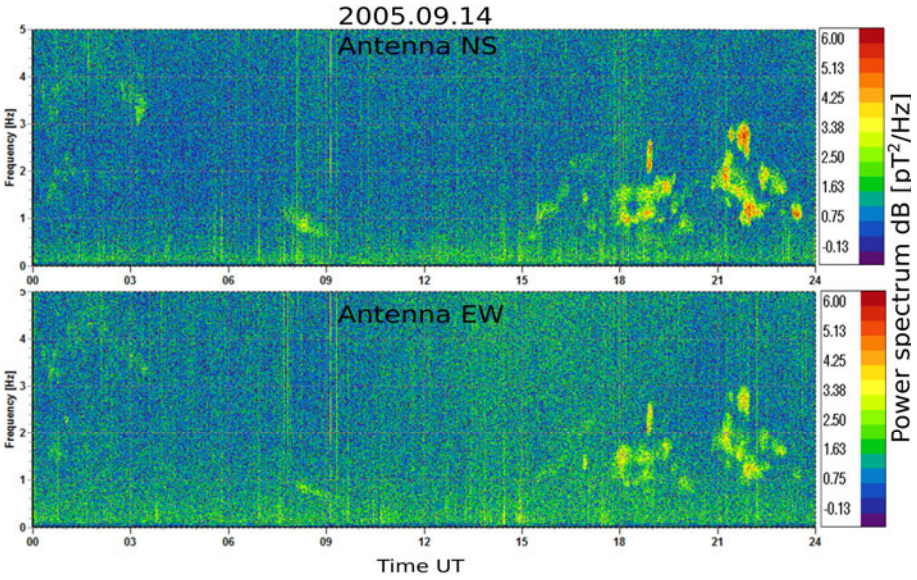

Fig. 4. The example of geomagnetic continuous pulsations (Pc1). The dynamic power spectrum is calculated on the basis of signals from NS (top panel) and EW (bottom panel) antennae collected on 14 September 2005 by the Hylaty ELF station.

irregular (Pi1). As a result, regular and irregular signals in the frequency band below 5 Hz can be observed on the Earth's surface (Kangas *et al.* 1998).

Figure 4 presents the dynamic power spectrum in the frequency range (0.03-5 Hz) for 14 September 2005 collected by the ELF station through NS and EW antennae. Geomagnetic continuous pulsations (Pc1) below 5 Hz are visible at different times during this day. The most intense Pc1 structures are observed at 18:00-24:00 UT. The Pc1 are generally more intense in the NS antenna than the EW, which is also demonstrated through differences between the NS spectrum (top panel) and the EW spectrum (bottom panel) seen in Fig. 4.

3.2 The Spectral Resonance Structures (SRS)

This is a type of signal that can also be observed in the ULF/ELF range below 5 Hz, due to ionospheric Alfvén resonator (IAR) excitation by negative-polarity cloud-to-ground (C-G) discharges whose polarity is that of the charge in the region in which the lightning leaders originated. In a similar manner, intense continuing currents associated with +CG discharges could also trigger IAR (Shalimov and Bösinger 2008). As a result of this excitation, the magnetic coils installed on the Earth's surface register signals containing spectral resonance structures (SRS). Occasionally these are also observed during winter thunderstorms in sprite-producing power spectra (Surkov *et al.* 2010). The SRS are mainly evident during night-time, independent of season, at different latitudes (Bösinger *et al.* 2002, Hebden *et al.* 2005, Odzimek *et al.* 2006, Semenova and Yahnin 2008).

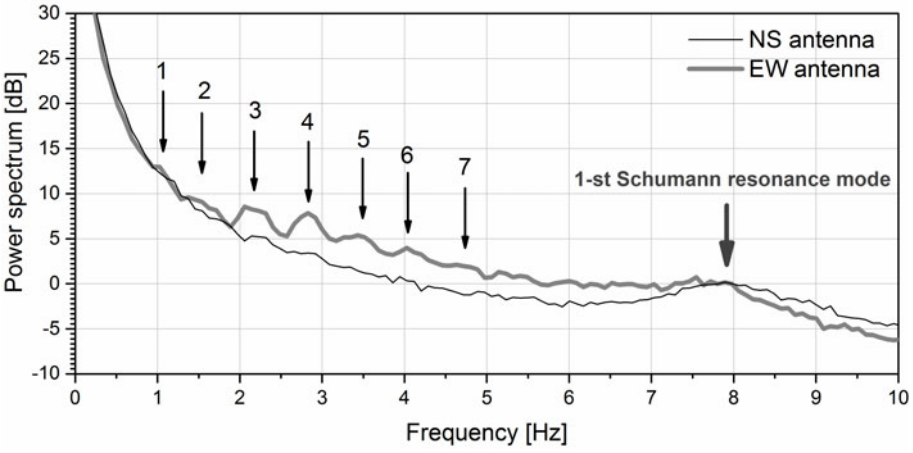

Fig. 5. The power spectrum calculated from ELF signals collected from 18:00 to 19:00 UT by the Hylaty ELF station on 24 September 2005. The seven peaks of the SRS are shown.

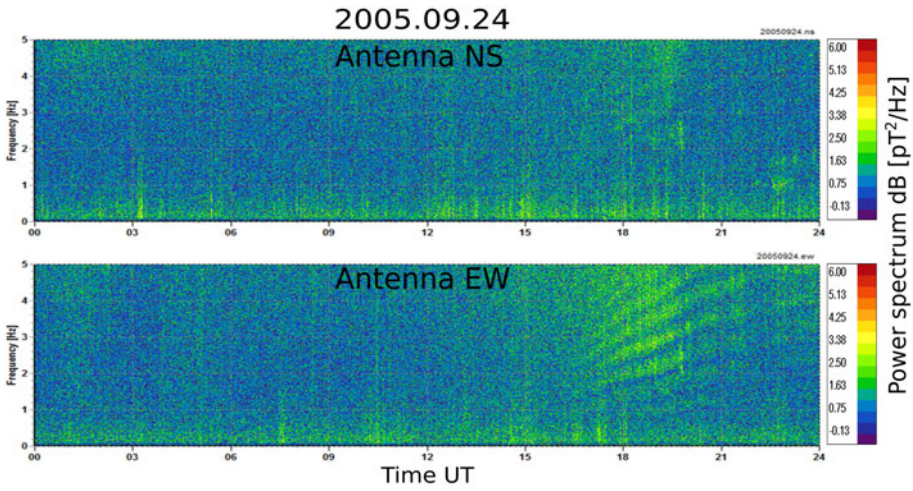

Fig. 6. The example of spectral resonance structures (SRS). The dynamic power spectrum of ELF signals is calculated on the basis of signals from NS (top panel) and EW (bottom panel) antennae collected by the Hylaty ELF station on 24 September 2005.

The SRS related to the Earth's ionosphere conductivity profile is shown in Fig. 5 as seven peaks in the power spectrum, and in Fig. 6 in which the dynamic power spectrum calculated for 24 September 2005 is presented. In the case of this particular day, we can see the most intense phenomena between 17:00 and 21:00 UT in the EW antenna (bottom panel).

3.3 Schumann resonance (SchR)

In many papers published over the last three decades, Schumann resonance phenomena have been used as a special diagnostic method for climate studies (Williams 2005). The growth in the number of studies was initiated by a paper about the connection between tropical air temperature and the intensity of Schumann resonance phenomena (Williams 1992). The Earth's surface and its ionosphere reflect electromagnetic (EM) waves in the extremely low frequency range of 3-3000 Hz (known as ELF) well. A resonant spherical cavity is thus formed in which electromagnetic waves propagate. This effect was theoretically predicted by Schumann (1952) but the first observation was made by Balser and Wagner (1960).

The strongest sources of ELF signals are lightning discharges in this cavity and these are sources of EM waves with a flat (for ELF range) and wide frequency range. The Schumann resonance is a natural phenomenon generally always visible on the power spectrum. For data from the Hylaty station, seven peaks of Schumann resonance can be found in both panels of Fig. 7 at:

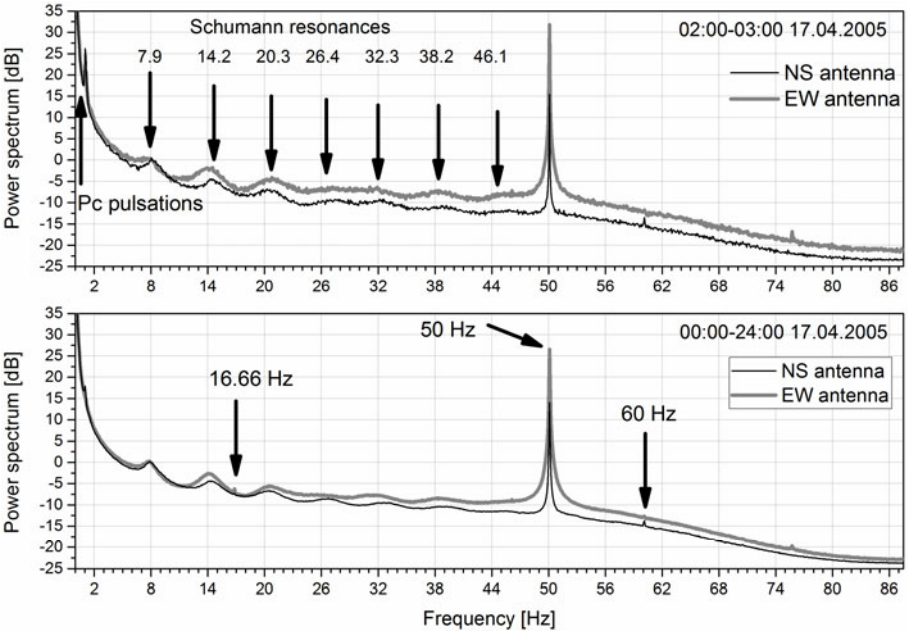

Fig. 7. The power spectrum is calculated based on ELF signals collected by the Hylaty ELF station on 17 April 2005. The top and bottom panels present the hourly (02:00-03:00 UT) and daily average power spectrum, respectively.

7.9, 14.2, 20.3, 26.4, 32.3, 38.2, and 46.1 Hz, respectively. Peak number eight of this phenomenon is masked by a strong peak at 50 Hz in the power spectrum. The next peaks are cut off by the anti-aliasing filter used at this station.

Figure 8 illustrates the dynamic power spectrum with colour-coding of amplitudes of signals with specific frequencies (vertical axis) and time (horizontal axis). The strong horizontal smudges/stripes that span the whole 24-hour periods correspond to subsequent Schumann resonances. In this particular figure, they are especially pronounced for the first three SchR modes, *i.e.*, 7.9, 14.2, 20.3 Hz. The changing intensity/colour of the smudges corresponds to SchR peak amplitude.

Daily changes in the intensity of Schumann resonance peaks are visible in Fig. 8, *e.g.*, in EW antenna it is maximum during UT afternoon hours. Information contained in the amplitudes of the SchR peaks allows one to study global and continental thunderstorm activity (Nieckarz *et al.* 2009, Dyrda *et al.* 2014). In the meantime, the analysis of frequency changes permits the study of the condition of the Earth-ionosphere cavity (Sátori *et al.* 2007) and its changes due to exposure to the Sun (Kulak *et al.* 2003, Sátori *et al.* 2005).

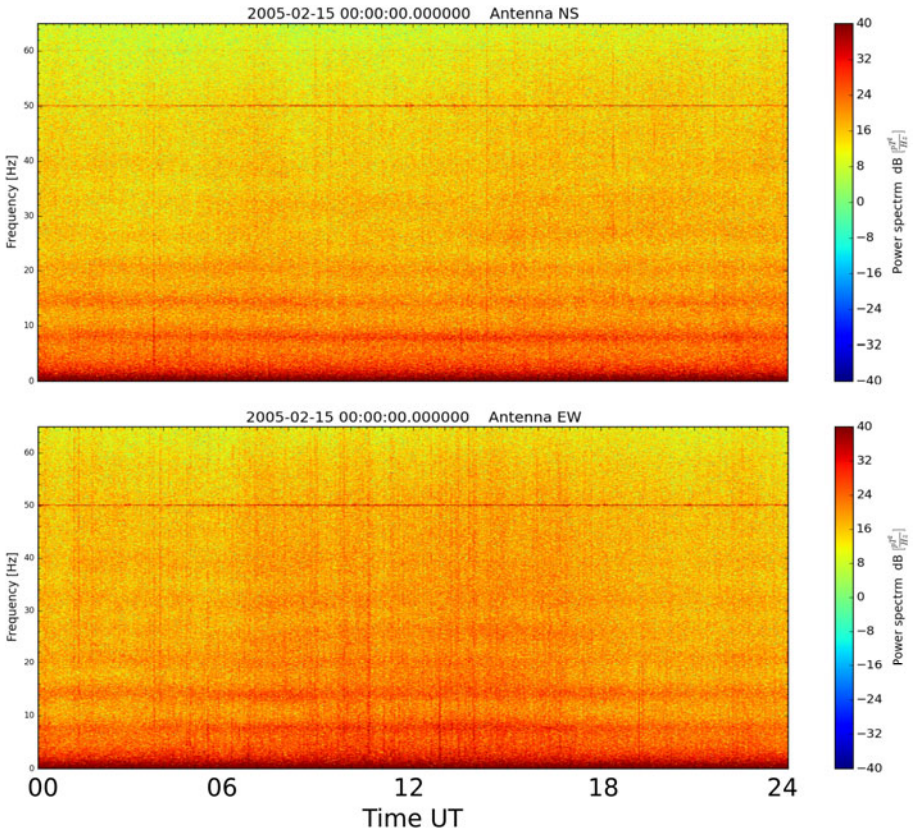

Fig. 8. The dynamic power spectrum of ELF signals is calculated on the basis of signals from NS (top panel) and EW (bottom panel) antennae collected on 15 Feb 2005 at the Hylaty ELF station. See text for details.

4. RESULTS

The most common method for assessing the occurrence of phenomena in the recorded signals, especially for studying the resonance phenomena, is the power spectrum (PS) calculated using the Fast Fourier Transform algorithm (FFT). An example of a PS recorded at the Hylaty ELF station is shown in Fig. 7. The narrow spectral lines, which are results of human activity, are clearly visible in this spectrum and are indicated by the arrows on the bottom panel.

The daily average PS was analysed. The assessment of the anthropogenic line activity was performed using three kinds of indices, AN, BG, and RLB, where AN is a net amplitude of the analysed narrow spectral line calculated as this line's amplitude read directly from the spectrum minus the spectral

amplitude identified in the nearest background of this line and marked BG. RLB is an index defined as the ratio of line's net amplitude (AN) to the nearest background amplitude (BG), which can be recorded with the formula RLB = AN/BG. It was possible to calculate the indices AN, BG and RLB, each for the three spectral lines, 16.66, 50, and 60 Hz, respectively. These indices were independently computed for each of the NS and EW antennae.

Indices AN50, BG50, and RLB50 are presented in Fig. 9 for both antennae, NS and EW, during the years 2005-2014. No significant linear trend in time domain is observed for any of the indices. There is, however, a seasonal variation.

A narrow spectral peak at 50 Hz, which predominantly originates from the Polish and European power grids, is always clearly visible. The values of the AN50 index calculated for both antennae are illustrated on the top panel in Fig. 9. Both $AN50_{NS}$ and $AN50_{EW}$ indices have two seasonal maximums, in winter and summer, even if they are neither very distinct in each year nor simultaneous on all antennae. The index $AN50_{EW}$ is always larger than $AN50_{NS}$ during the entire period of study.

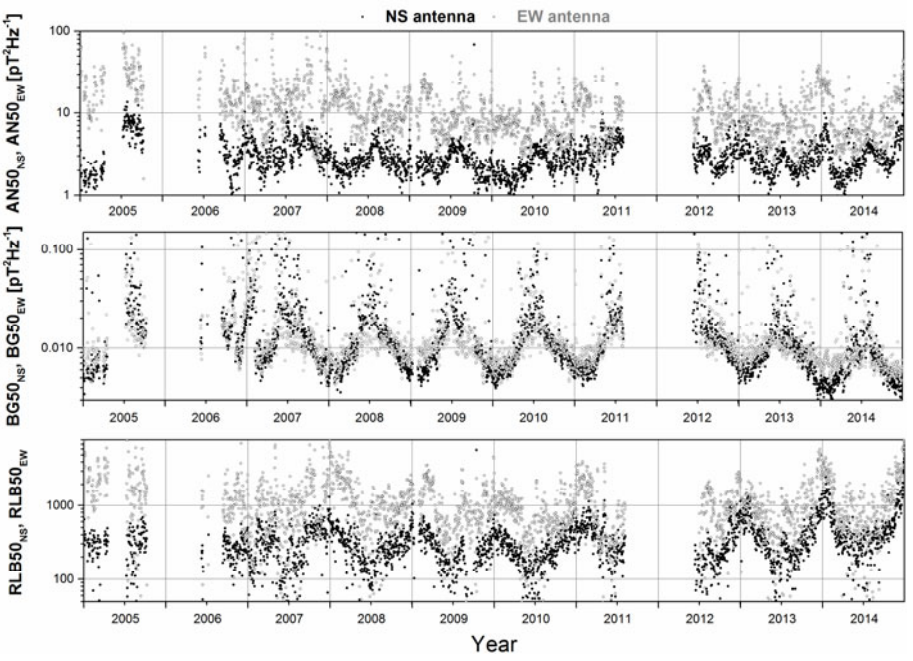

Fig. 9. The variability of indices: AN50 (top panel), BG50 (middle panel), and RLB50 (bottom panel) at both antennae during the years 2005-2014. The results are not available in certain periods due to technical problems.

On both antennae, the timeline of the BG50 index displays strong and repeatable seasonal variability with a single peak in summer and a single trough in winter. Values of the $BG50_{NS}$ and $BG50_{EW}$ indices strongly correspond with the amplitude of Schumann resonances in this range of the power spectrum (see Fig. 7). It is generally known from observations that resonance amplitudes depend on the intensity of the global thunderstorm activity (*i.e.*, the frequency of discharges, amplitudes of discharge currents and on the length of discharge channels) and on the distance between thunderstorm areas and the ELF station (Kulak *et al.* 2006), even if these dependencies are not linear. In a simplified approach, the values of the BG50 indices from both antennae provide an approximated picture of the global thunderstorm activity and in terms of its nature is compatible with the current state of research in this area. Different types of global thunderstorm activity observation indicate that the northern hemisphere is much more active than the southern counterpart (Christian *et al.* 2003). This is explained by the asymmetrical distribution of landmass and the resulting tracts of humidity and air circulation around the globe. Notably, tropical landmass provides the greatest contribution to global thunderstorm activity (Williams 2005).

The RLB50 index, defined as the AN to BG ratio, was devised to provide quantitative assessment of the contribution from the anthropogenic 50 Hz spectral line to the amplitude of the natural signal in this part of the spectrum. As a result, it was observed that while both RLB50 indices are higher in winter than in summer, the $RLB50_{EW}$ variety is always greater than $RLB50_{NS}$ across the study period. It is worth noting that the location of the 50 Hz peak in the frequency domain corresponds with the location of the eighth mode of Schumann resonance (around 51.5 Hz). It should also be noted that more than ten modes could be observed (Fullekrug 2005) when using a very wide band receiver.

The spectral line 60 Hz, which is mainly characteristic of the North American power grids, is weakly visible in datasets recorded at the Hylaty station. Usually it is only the average power spectrum produced for a longer period of time (more than 30 min) that enables spectral lines to be observed. It should be noted that the frequency of 60 Hz is in the top part of the declining transmission characteristics of station (see Fig. 7), but it is strong enough to study its behaviour in the period analysed. Figure 10 presents an analysis of variability of the indices AN60, BG60, and RLB60 during the years 2005-2014 for each of the NS and EW antennae. Both AN60 indices display seasonality with peaks in winter and summer with the former peak normally better isolated than the latter. The $AN60_{NS}$ index is greater than $AN60_{EW}$ across the study period. The pattern of the BG60 index in time has the same origin and a nearly identical shape to BG50. The only significant difference is the low values of BG60 due to the partial suppression of this spectrum range

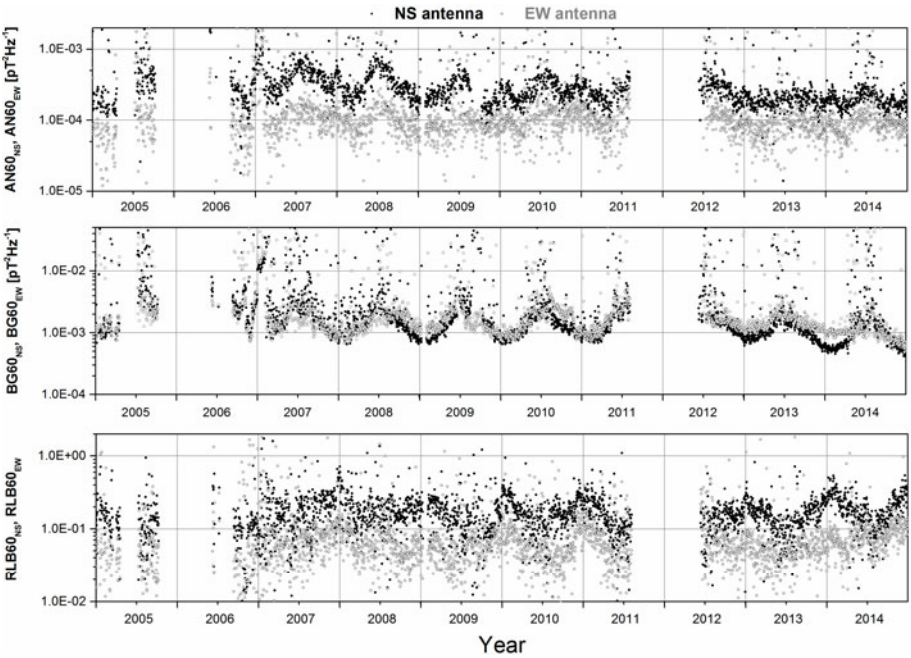

Fig. 10. The variability of indices: AN60 (top panel), BG60 (middle panel), and RLB60 (bottom panel) at both antennae during the years 2005-2014. The results are not available in certain periods due to technical problems.

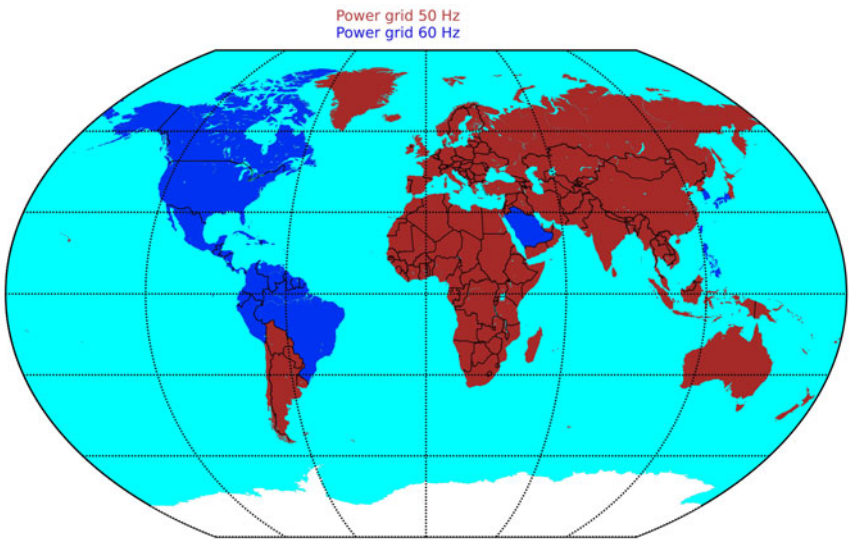

Fig. 11. The world map of electrification systems based on Hughes (1983) and Neidhofer (2011). The brown colour indicates the area where power lines use a frequency equal to 50 Hz and the navy colour indicates the areas powered by 60 Hz.

by the station's filter. The lower panel in Fig. 10 depicts the timeline of the $RLB60_{NS}$ and $RLB60_{EW}$ indices during the years 2005-2014. Any significant linear trend in time domain is observed for either index, but seasonal variations are present. In winter both indices are higher than in the summer period but always index $RLB60_{NS}$ is bigger than $RLB60_{EW}$. Index $RLB60_{NS}$ is, on average, 6.9 times larger than $RLB60_{EW}$.

It is known that different countries use different voltages and one of two values for the frequency of the power grid. The use of frequencies in the power systems of the World is presented in Fig. 11. The national power grids around the globe operate at frequencies equal to 50 or 60 Hz (Hughes 1983, L'Abbate *et al.* 2007, Neidhofer 2011).

The minor spectral lines at 16.66 Hz are poorly visible (see Fig. 7). The variability of the AN16, BG16, and RLB16 indices for both antennae during the study period is presented in Fig. 12. The timeline of the AN16 index from both antennae reveals no clear seasonality. During the period 2007-2009, $AN16_{EW}$ was systematically greater than $AN16_{NS}$, while for the rest of the period the two are approximately equal. Also in this case, the timelines of both BG16 varieties have the same origin and a nearly identical nature to their BG50 counterparts.

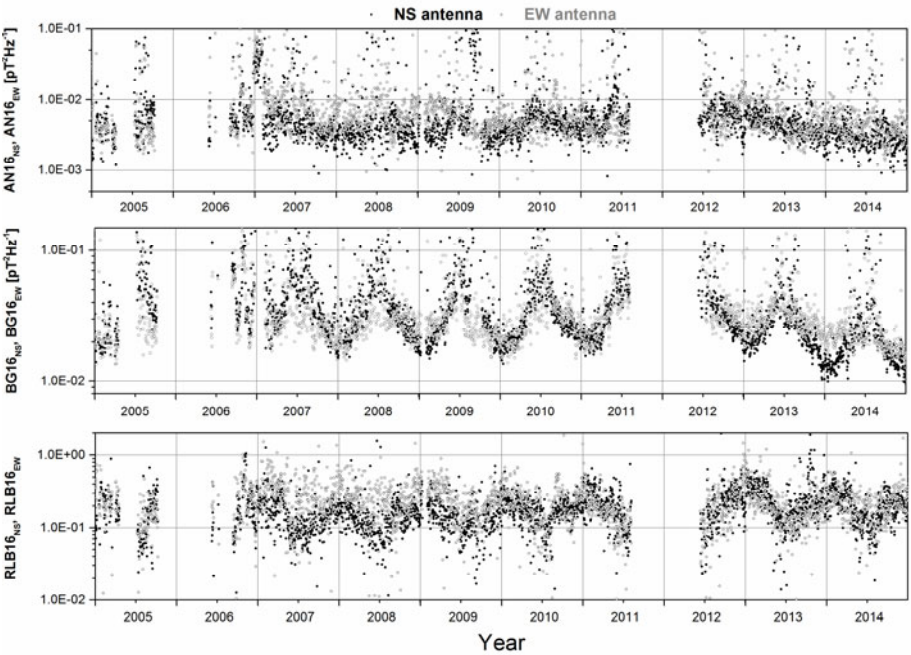

Fig. 12. The variability of indices: AN16 (top panel), BG16 (middle panel), and RLB16 (bottom panel) at both antennae during the years 2005-2014. The results are not available in certain periods due to a technical problem.

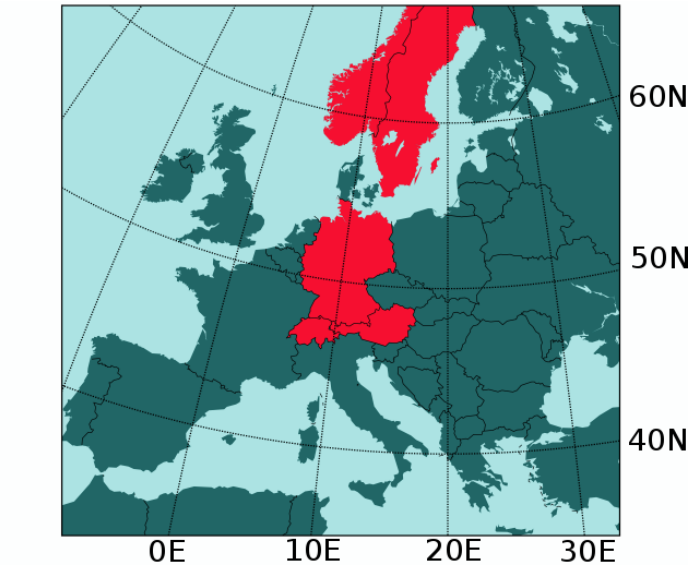

Fig. 13. A map of the electrification systems for European railways (based on Frey 2012). European electric rail tractions operate at DC voltage and AC 50 Hz voltage (blue) as well as AC 16.66 Hz (red).

The seasonal variability of both indices, $RLB16_{NS}$ and $RLB16_{EW}$, is observed. Again, both indices are higher in winter than in summer. In the period 2007-2009, $RLB16_{EW}$ is slightly greater than $RLB16_{NS}$ on a permanent basis. In the rest of the period, both indices are comparable. Generally, the amplitudes of the line spectrum 16.66 Hz in a dataset collected at the Hylaty station are small and vary in time. It is known that this line comes from several European railway systems: Germany, Austria, Switzerland, Sweden, and Norway (Frey 2012). Figure 13 shows a map of the electrification systems of railways in Europe. It is noticeable that the Austrian railway network, with that frequency system, is close to that in the southeast corner of Poland where the Hylaty ELF station is located.

5. CONCLUSIONS

The amplitudes of all anthropogenic spectral lines (16.66, 50, and 60 Hz) are stable over a long time scale. Unexpected disorders that affect the quality of measurements were not observed. This means that the Bieszczady mountains are a good location for this type of measurement. The regular seasonal intermittency is visible in almost all BG, AN50, AN60, and RLB indices.

However, the anthropogenic lines are narrow spectral lines but could disturb the observed natural power spectrum of Schumann resonances. When

there is an enormous intensity of these lines, the analysis of Schuman resonances is impossible. Generally, the index $AN50_{EW}$ is greater than $AN60_{NS}$, whereas the index $AN60_{NS}$ is higher than $AN60_{EW}$ in all study periods.

In the Bieszczady mountains the relatively low amplitude of the spectral lines 50 and 60 Hz permits us to study around 6-7 peaks of Schumann resonance effectively. Because the train power line 16.66 Hz is not strong, analysis of the 2nd (~14 Hz) peak of Schuman resonance is also possible at all times. The problem with the huge amplitude of the train power lines is demonstrable in those regions where railways are supplied via 16.66 Hz, which includes Germany, Switzerland, Austria, Sweden, Norway and the immediate borders of these countries (see Fig. 13). For example, this problem exists in ELF recordings in the Nagycenk (Hungary) observatory close to the Austrian border. In consequence, special stop-band filters have been used in the recording system (Sátori *et al.* 1996).

Intensive human activity imposes strong constraints on the spatial opportunities for locating stations. It is clearly visible that the correct choice of location for an ELF station is important and has a strong influence on the quality of magnetic measurements for geophysical purposes.

Acknowledgments. The paper was partially financed by the National Science Centre (NCN, Poland) grants NCN-2012/04/M/ST10/00565 and N N306 039040, and also grant financed by the Jagiellonian University No. WFAIS-FOCUS 139/F/ZN/2016.

References

Balser, M., and C.A. Wagner (1960), Observations of Earth-ionosphere cavity resonances, *Nature* **188**, 4751, 638-641, DOI: 10.1038/188638a0.

Beggan, C.D., T. Gabillard, A. Swan, S. Flower, and A. Thomson (2012), Investigation of global lightning using Schumann resonances measured by high frequency induction coil magnetometers in the UK. **In:** *AGU Fall Meeting, Lightning and Atmospheric Electricity in Thunderstorms V, San Francisco, USA*, AE23B-0333.

Bezrodny, V., O. Budanov, A. Koloskov, M. Hayakawa, V. Sinitsin, Y. Yampolski, and V. Korepanov (2007), The ELF band as a possible spectral window for seismo-ionospheric diagnostics, *Sun Geosphere* **2**, 2, 88-95.

Bösinger, T., C. Haldoupis, P.P. Belyaev, M.N. Yakunin, N.V. Semenova, A.G. Demekhov, and A.V. Angelopoulus (2002), Spectral properties of the ionospheric Alfvén resonator observed at a low-latitude station (L = 1.3), *J. Geophys. Res.* **107**, A10, SIA4-1 – SIA4-9, DOI: 10.1029/2001JA005076.

Christian, H.J., R.J. Blakeslee, D.J. Boccippio, W.L. Boeck, D.E. Buechler, K.T. Driscoll, S.J. Goodman, J.M. Hall, W.J. Koshak, D.M. Mach, and M.F. Stewart (2003), Global frequency and distribution of lightning as observed from space by the optical transient detector, *J. Geophys. Res.* **108**, D1, 4005, DOI: 10.1029/2002JD002347.

Dyrda, M., A. Kulak, J. Mlynarczyk, M. Ostrowski, J. Kubisz, A. Michalec, and Z. Nieckarz (2014), Application of the Schumann resonance spectral decomposition in characterizing the main African thunderstorm center, *J. Geophys. Res. Atmos.* **119**, 23, 13338-13349, DOI: 10.1002/2014JD022613.

Engebretson, M.J., M.R. Lessard, J. Bortnik, J.C. Green, R.B. Horne, D.L. Detrick, A.T. Weatherwax, J. Manninen, N.J. Petit, J.L. Posch, and M.C. Rose (2008), Pc1-Pc2 waves and energetic particle precipitation during and after magnetic storms: Superposed epoch analysis and case studies, *J. Geophys. Res*. **113**, A1, A01211, DOI: 10.1029/2007JA012362.

Fraser-Smith, A.C., and R.A. Helliwell (1994), Overview of the Stanford University/Office of Naval Research ELF/VLF radio noise survey. **In**: J.M. Goodman (ed.), *Proc. 1993 Ionospheric Effects Symposium, SRI International, Arlington, Virginia*, 502-509.

Frey, S. (2012), *Railway Electrification System and Engineering*, White Word Publications.

Fullekrug, M. (2005), Detection of thirteen resonances of radio waves from particularly intense lightning discharges, *Geophys. Res. Lett.* **32**, 13, L13809, DOI: 10.1029/2005GL023028.

Hebden, S.R., T.R. Robinson, D.M. Wright, T. Yeoman, T. Raita, and T.A. Bösinger (2005), Quantitative analysis of the diurnal evolution of ionospheric Alfvén resonator magnetic resonance features and of changing IAR parameters, *Ann. Geophys*. **23**, 5, 1711-1721.

Hobara, Y., N. Iwasaki, T. Hayashida, T. Tsuchiya, E.R. Williams, M. Sera, Y. Ikegami, and M. Hayakawa (2000), New ELF observation site in Moshiri, Hokkaido, Japan, and the results of preliminary data analysis, *J. Atmos. Electr.* **20**, 2, 99-109.

Hughes, T.P. (1983), *Networks of Power: Electrification in Western Society 1880-1930*, The Johns Hopkins University Press, Baltimore.

Jankowski, J., and C. Sucksdorff (1996), *Guide for Magnetic Measurements and Observatory Practice*, International Association of Geomagnetism and Aeronomy, Warsaw, Poland.

Kangas, J., A. Guglielmi, and O. Pokhotelov (1998), Morphology and physics of short-period magnetic pulsations, *Space Sci. Rev.* **83**, 3, 435-512, DOI: 10.1023/A:1005063911643.

Kulak, A., S. Zieba, S. Micek, and Z. Nieckarz (2003), Solar variations in extremely low frequency propagation parameters: 1. A two-dimensional telegraph equation (TDTE) model of ELF propagation and fundamental parameters of

Schumann resonances, *J. Geophys. Res*. **108**, A7, 1270, DOI: 10.1029/2002JA009304.

Kulak, A., J. Mlynarczyk, S. Zieba, S. Micek, and Z. Nieckarz (2006), Studies of ELF propagation in the spherical shell cavity using a field decomposition method based on asymmetry of Schumann resonance curves, *J. Geophys. Res*. **111**, A10, A10304, DOI: 10.1029/2005JA011429.

Kulak, A., J. Kubisz, S. Klucjasz, A. Michalec, J. Mlynarczyk, Z. Nieckarz, M. Ostrowski, and S. Zieba (2014), Extremely low frequency electromagnetic field measurements at the Hylaty station and methodology of signal analysis, *Radio Sci*. **49**, 6, 361-370, DOI: 10.1002/2014RS005400.

L'Abbate, A., G. Fulli, F. Starr, and S.D. Peteves (2007), Distributed power generation in Europe: Technical issues for further integration, *JCR Sci. Tech. Reports*, European Commission, EUR 23234.

Love, J., and A. Chulliat (2013), An international network of magnetic observation, *EOS* **94**, 42, 373-384.

Neidhofer, G. (2011), 50-Hz frequency [history]: how the standard emerged from a European jungle, *IEEE Power Energy Mag.* **9**, 4, 66-81, DOI: 10.1109/MPE.2011.941165.

Neska, M., and G. Sátori (2006), Schumann resonance observation at Polish Polar Station at Spitsbergen and in Central Geophysical Observatory in Belsk, Poland, *Prz. Geofiz*. **3-4**, 189-198 (in Polish).

Nieckarz, Z., S. Zięba, A. Kułak, and A. Michalec (2009), Study of the periodicities of lightning activity in three main thunderstorm centers based on Schumann resonance measurements, *Month. Weath. Rev.* **137**, 12, 4401-4409, DOI: 10.1175/2009MWR2920.1.

Odzimek, A., A. Kulak, A. Michalec, and J. Kubisz (2006), An automatic method to determine the frequency scale of the ionospheric Alfven resonator using data from Hylaty station, Poland, *Ann. Geophys*. **24**, 8, 2151-2158.

Price, C., M. Finkelstein, B. Starobinets, and E. Williams (1999), A new Schumann resonance station in the Negev desert for monitoring global lightning activity. **In:** *Proc. 11th Int. Conf. on Atmospheric Electricity, 7-11 June 1999, Guntersville, Alabama*, NASA, Marshall Space Flight Center, Alabama, 695-697.

Salazar, A. (2006), Energy propagation of thermal waves, *Eur. J. Phys.* **27**, 6, 1349-1355, DOI: 10.1088/0143-0807/27/6/009.

Sátori, G., J. Szendroi, and J. Vero (1996), Monitoring Schumann resonances – I. Methodology, *J. Atmos. Sol. Terr. Phys*. **58**, 13, 1475-1481, DOI: 10.1016/0021-9169(95)00145-X.

Sátori, G., E.R. Williams, and V. Mushtak (2005), Response of the Earth-ionosphere cavity resonator to the 11-year solar cycle in X-radiation, *J. Atmos. Sol. Terr. Phys*. **67**, 6, 553-562, DOI: 10.1016/j.jastp.2004.12.006.

Sátori, G., M. Neska, E. Williams, and J. Szendroi (2007), Signatures of the day-night asymmetry of the Earth-ionosphere cavity in high time resolution Schumann resonance records, *Radio Sci*. **42**, 2, RS2S10, DOI: 10.1029/2006RS003483.

Schumann, W.O. (1952), On the free oscillation of a conducting sphere, which is surrounded by an air layer and an ionospheric shell, *Z. Naturforsch.* **7a**, 149-154 (in German).

Semenova, N.V., and A.G. Yahnin (2008), Diurnal behaviour of the ionospheric Alfven resonator signatures as observed at high latitude observatory Baentsburg, *Ann. Geophys*. **26**, 8, 2245-2251.

Shalimov, S., and T. Bösinger (2008), On distant excitation of the ionospheric Alfvén resonator by positive cloud-to-ground lightning discharges, *J. Geophys. Res.* **113**, A2, A02303, DOI: 10.1029/2007JA012614.

Surkov, V.V., Y. Matsudo, M. Hayakawa, and S.V. Goncharov (2010), Estimation of lightning and sprite parameters based on observation of sprite-producing lightning power spectra, *J. Atmos. Sol. Terr. Phys*. **72**, 5-6, 448-456, DOI: 10.1016/j.jastp.2010.01.001.

Turbitt, C., J. Matzka, J. Rasson, B. St-Louis, and D. Stewart (2013), An instrument performance and data quality standard for intermagnet one-second data exchange. **In:** *Proc. 15th IAGA Workshop on Geomagnetic Observatory Instruments, Data Acquisition and Processing*, No. 03/13, 186-188.

Williams, E.R. (1992), The Schumann resonance: A global tropical thermometer, *Science* **256**, 5060, 1184-1187, DOI: 10.1126/science.256.5060.1184.

Williams, E.R. (2005), Lightning and climate: A review, *Atmos. Res.* **76**, 1-4, 272-287, DOI: 10.1016/j.atmosres.2004.11.014.

Received 20 January 2016
Received in revised form 13 May 2016
Accepted 15 June 2016